Accepted Manuscript

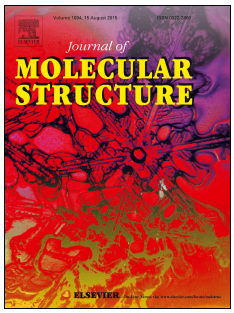

Reactive, spectroscopic and antimicrobial assessments of 5-[(4-methylphenyl) acetamido]-2-(4-*tert*-butylphenyl)benzoxazole: Combined experimental and computational study

Y. Sheena Mary, Nourah Z. Alzoman, Vidya V. Menon, Ebtehal S. Al-Abdullah, Ali A. El-Emam, C. Yohannan Panicker, Ozlem Temiz-Arpaci, Stevan Armaković, Sanja J. Armaković, C. Van Alsenoy

PII: S0022-2860(16)30951-6

DOI: 10.1016/j.molstruc.2016.09.024

Reference: MOLSTR 22936

To appear in: *Journal of Molecular Structure*

Received Date: 5 August 2016

Revised Date: 8 September 2016

Accepted Date: 8 September 2016

Please cite this article as: Y.S. Mary, N.Z. Alzoman, V.V. Menon, E.S. Al-Abdullah, A.A. El-Emam, C.Y. Panicker, O. Temiz-Arpaci, S. Armaković, S.J. Armaković, C. Van Alsenoy, Reactive, spectroscopic and antimicrobial assessments of 5-[(4-methylphenyl) acetamido]-2-(4-*tert*-butylphenyl)benzoxazole: Combined experimental and computational study, *Journal of Molecular Structure* (2016), doi: 10.1016/j.molstruc.2016.09.024.

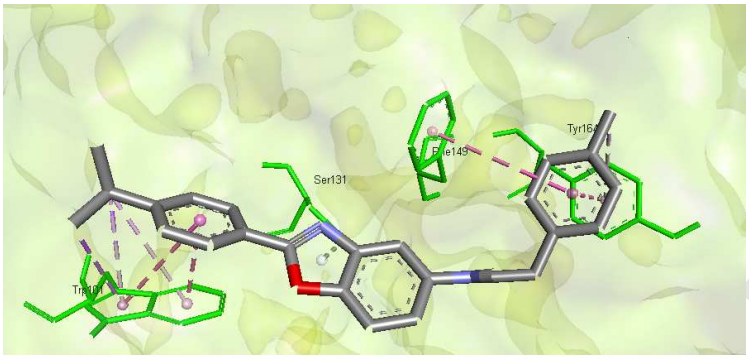

Reactive, spectroscopic and antimicrobial assessments of 5-[(4-methylphenyl) acetamido]-2-(4-tert-butylphenyl)benzoxazole: Combined experimental and computational study

Sheena Mary Y[a*], Nourah Z. Alzoman[b], Vidya V.Menon[c,d], Ebtehal S. Al-Abdullah[b], Ali A. El-Emam[b], C.Yohannan Panicker[a], Ozlem Temiz-Arpaci[e] , Stevan Armaković[f], Sanja J. Armaković[g], C.Van Alsenoy[h]

[a]Department of Physics, Fatima Mata National College, Kollam, Kerala, India

[b]Department of Pharmaceutical Chemistry, College of Pharmacy, King Saud University, Riyadh 11451, Saudi Arabia

[c]Department of Physics, IES College of Engineering, Chittilappily, Thrissur, Kerala, India

[d]RD, Bharathiar University, Coimbatore, Tamilnadu, India

[e]Ankara University Faculty of Pharmacy, Department of Pharmaceutical Chemistry, TR-06100, Tandogan, Ankara, Turkey

[f] University of Novi Sad, Faculty of Sciences, Department of Physics, Trg D. Obradovića 4, 21000 Novi Sad, Serbia

[g]University of Novi Sad, Faculty of Sciences, Department of Chemistry, Biochemistry and Environmental Protection, Trg D. Obradovića 3, 21000 Novi Sad, Serbia

[h]Department of Chemistry, University of Antwerp, Groenenborgerlaan 171, B-2020, Antwerp, Belgium

*author for corresponence email: sypanicker@rediffmail.com

Abstract

The synthesis, FT-IR, FT-Raman and NMR spectral analysis of an antimicrobial active benzoxazole derivative, 5-[(4-methylphenyl)acetamido]-2-(4-tert-butylphenyl) benzoxazole (MPATB) is reported. The localization of HOMO, LUMO plots in the title compound over the title molecule shows the charge transfer in the molecular system through the conjugated paths.The electrophilic and nucleophilic sites are revealed from the molecular electrostatic potential map. The first hyperpolarizability of the title compound is greater than that of the standard nonlinear optical material urea and the title

compound and its derivatives are good objects for further research in nonlinear optical analysis. Molecule sites prone to electrophilic attacks have been detected by calculation of average local ionization energies, while calculations of Fukui functions have provided additional information about the local reactivity properties. Bond dissociation energies have been calculated in order to investigate autoxidation possibilities of the title molecule, as well as to determine the weakest bonds and therefore the sites where process of degradation could start. Reactive properties with water have been investigated by molecular dynamics simulations and calculations of radial distribution functions. The compound possessed broad spectrum activity against all of the tested Gram-positive and Gram-negative bacteria and yeasts, their minimum inhibitory concentrations ranging between 8-128 μg/ml. The compound exhibited significant antifungal activity (64μg/ml) against *Candida krusei*, at same potency with the compared standard drugs fluconazole. The docked title compound forms a stable complex with thymidylate synthase and got a binding affinity value of -8.5kcal/mol and the title compound can be a lead compound for developing new anti-cancerous drug.

Keywords: Benzoxazole; DFT; ALIE; BDE; Molecular docking.

1. Introduction

Heterocyclic compounds such as benzoxazoles have attracted attention due to their diverse pharmacological and biological properties like antibacterial, antifungal, anti-tubercular, anti-tumor and antiviral [1-6]. Benzoxazoles are the structural bio-isoesters of nucleotides such as guanine and adenine and they interact easily with biopolymers of living system [7, 8] and they inhibit essential bacterial enzymes, such as hyaluronanlyase [9] and isocitratelyase [10] as well as bacterial two component systems [11, 12]. Mabied et al. [13] reported the crystal structure of stereochemistry study of 2-substituted benzoxazole derivatives and Jayana et al. [14] reported the synthesis, antibacterial and antioxidant evaluation of novel 1-(5,7-dichloro-1,3-benzoxazol-2-yl)-1H-pyrazolo[3,4-b] quinoline derivatives.

Studies of reactive properties of newly synthetized organic molecules with potential important biological activities are very important for the development and improvement of methods for water purification. Namely, molecules that are active components of pharmaceutical products are synthetized to be very stable, thus natural

conditions and conventional purification methods are not enough effective for their degradation [15-17.]

Unfortunately, due to various reasons drugs are entering the environment and are accumulating especially in the water resources, where they are toxic to aquatic organisms. So far these types of compounds have been detected in all types of waters [18]. Fortunately, advanced oxidation processes are seen as the alternative when it comes to the degradation of these compounds [19-21]. Forced degradation experiments are very important in the process of making of new pharmacological formulations [22]. These experiments serve as tools by which it is possible to evaluate degradation mechanisms and toxicity. These experiments are expensive and tedious, but principles of molecular modeling are very useful for their rationalization. In this regard it is important to note that DFT calculations and MD simulations are able to provide important reactive properties thanks to which autoxidation and hydrolysis properties can be effectively initially assessed. Taking this into account in this work we have also been devoted to the investigation of specific local reactivity properties based on DFT calculations and MD simulations.

2. Experimental

2.1 Materials and methods

The chemicals and solvents were purchased from Sigma-Aldrich (Munich, Germany) and Fisher Scientific (Pittsburgh, PA, USA); they were used without purification. Silica gel HF_{254} chromatoplates (0.3 mm) were used for thin layer chromatography, and the mobile phase was chloroform/methanol (10:0.5). Melting point was recorded on a Stuart Scientific SMP1 instrument (Bibby Scientific Limited, Staffordshire, UK) and is uncorrected. NMR spectra were recorded on a Varian Mercury 400 MHz NMR spectrometer (Palo Alto, CA, USA); trimethylsilane (TMS) was used as an internal standard. The mass spectra was recorded on a Waters ZQ Micromass LC-MS spectrometer (Milford, MA, USA) using the ESI(+) method.

The FT-IR spectrum (Fig. S1-supporting material) was recorded using KBr pellets on a DR/Jasco FT-IR 6300 spectrometer. The FT-Raman spectrum (Fig. S2-supporting material) was obtained on a Bruker RFS 100/s, Germany. For excitation of the spectrum the emission of Nd:YAG laser was used, excitation wavelength 1064 nm, maximal power

150 mW, measurement on solid sample. The spectral resolution after apodization was 2 cm^{-1}.

Materials used in the microbiology study were; Mueller Hinton agar (MHA) (Merck, Darmstadt, Germany), Mueller Hinton broth (MHB) (Merck), Sabouraud dextrose agar (SDA) (Merck), RPMI-1640 medium with L-glutamine (Sigma-Aldrich), 3-(*N*-morpholino)-propane-sulfonic acid (MOPS) (Sigma-Aldrich), 96-well micro plates (BD, Franklin Lakes, NJ, USA), ampicillin (Mustafa Nevzat Pharmaceuticals, Istanbul, Turkey), gentamycin sulfate (Paninkret Chem.-Pharm., Pinneberg, Germany), ofloxacin (Zhejiang Huangyan East Asia Chemical Co. Ltd., Huangyan, Zhejiang, China), vancomycin (Mayne Pharma, Salisbury South, SA, Australia), meropenem (Astra Zeneca, Istanbul, Turkey), fluconazole (Sigma-Aldrich), amphotericin B (Riedel de Haen, Seelze, Germany), isoniazid (Sigma-Aldrich), ethambutol (Sigma-Aldrich), DMSO (Riedel de Haen).

Microorganisms used in the assay were; *Klebsiella pneumoniae* clinical isolate (extended beta lactamase spectrum (ESBL)), *Escherichia coli* isolate (ESBL), *Enterococcus faecalis*isolate (resistant to vancomycin (VRE)), and *Staphylococcus aureus* isolate (resistant to methicilline (MRSA)), *K. pneumoniae* RSKK 574, *E. coli* ATCC 25922, *E. faecalis* ATCC 29212, *S. aureus* ATCC 29213, *Candida albicans* ATCC 10231, *Candida krusei* ATCC 6258, *Mycobacterium tuberculosis* H37RV ATCC 27294 and a clinical isolate of *M. tuberculosis*. Reference strains and clinical isolates were provided by Gazi University, Faculty of Pharmacy, Department of Pharmaceutical Microbiology, Culture Collection, Ankara, Turkey, and Gazi University Hospital Microbiology Laboratory, Ankara, Turkey, respectively.

2.2 *Chemistry*

General procedure for the preparation of 5-[(4-methylphenyl)acetamido]-2-(4-tert-butylphenyl)benzoxazole

Firstly, 5-amino-2-(4-tert-butylphenyl)-benzoxazole was synthesized by heating 0.02 mol 2,4-diaminophenol·2.HCl with 0.02mol 4-tert-butylbenzoic acid in 25 g polyphosphoric acid (PPA) and stirring for 3-4 h. At the end of the reaction period, the residue was poured into an ice/water mixture and the solution was neutralized with 10%

NaOH. The resulting precipitate was filtered, washed with distilled water, dissolved in boiling ethanol with 0.2 g charcoal, and filtered off. Then distilled water was added to the filtrate slowly in order to stimulate crystallization. The crude compound **3** was obtained by filtering and drying the crystalline material [2]. Then, 4-methylphenyl acetic acid (0.5 mmol) and thionylchloride (1.5 ml) were refluxed in benzene (5 ml) at 80°C for 3h. excess thionylchloride was removed *in vacuo*. The 4-methylphenyl acetic acid chloride **(5)** was dissolved in ether (10 ml) and this solution added during 1 h to a stirred, ice-cold mixture of 5-amino-2-[4-tert-butylphenyl]benzoxazole (**3) (**0.5 mmol), sodiumbicarbonate (0.5 mmol), diethylether (10 ml) and water (10 ml). The mixture was kept stirred overnight at room temperature and filtered. The precipitate was washed with water, 2M HCl and water, respectively and finally with ether to give compound. The product was re-crystallized from ethanol-water as needles which are dried *in vacuo*. (scheme).

2.3 *Microbiological assays*

For microbiological assays, standard powders of ampicillin, meropenem, gentamycin sulfate, ofloxacin, vancomycin, fluconazole, amphotericin B, isoniazid, and ethambutol were dissolved in appropriate solvents recommended by Clinical and Laboratory Standards Institute (CLSI) guidelines [23, 24]. Stock solutions of the test compounds were prepared in DMSO. Bacterial susceptibility testing was performed according to the guidelines of CLSI M100-S18 [24]. MHB was added to each well of the micro plates. The bacterial suspensions used for inoculation were prepared at 10^6 CFU/ml by diluting fresh cultures at McFarland 0.5 density. Suspensions of the bacteria at 10^6 CFU/ml were inoculated to the two-fold diluted solution of the compounds. A 10-µl bacterium inoculum was added to each well of the micro plates. There were 10^5 CFU/ml bacteria in the wells after inoculations. Micro plates were incubated at 37°C over night. Fungal susceptibility testing was performed according to the guidelines of CLSI M27-A3 [23]. RPMI-1640 medium with L-glutamine buffered to pH 7 with MOPS was added to each well of the micro plates. The colonies were suspended in sterile saline, and the resulting suspension was adjusted to McFarland 0.5 density. A working suspension was prepared by appropriate dilution of the stock suspension. A 10-µl bacterium inoculum was added to each well of the micro plates resulting in 10^3 CFU/ml yeasts in the wells.

Micro plates were incubated at 35°C for 24-48 hours. After incubation, the lowest concentration of the compounds that completely inhibited macroscopic growth was determined and reported as minimum inhibitory concentration (MIC). All solvents and diluents, pure microorganisms, and pure media were used in control wells. All experiments were done in three parallel series. The data on the antimicrobial activity of the compounds and the control drugs as MIC (µg/ml) values are given in table 1. The synthesized compound was found to possess MIC values between 8- 128 µg/ml for Mycobacterium tuberculosis, some Gram-negative, Gram-positive bacteria and their isolates and some fungi. The synthesized compound exhibited the same antifungal activity against *C. krusei* with MIC values of 64µg/ml with the tested reference drug fluconazole. However, all compounds showed lower antibacterial and anti-mycobacterial activity against the microorganisms than the control drugs.

3. Computational details

The molecular geometry optimization, polarizabilities and natural bond orbital analysis for the title compound are calculated by density functional using B3LYP/6-311++G(d,p) [25, 26] level of theory using Gaussian09 software [27]. The calculated scaled wave numbers are scaled by using scaling factor as reported in literature [28]. With the help of potential energy distribution analysis [29] and Gaussview program [30] the vibrational assignments were carried out. The optimized geometrical (Fig.1) parameters are given in table S1 (supporting material).

Jaguar 9.0 program [31], as implemented in Schrödinger Materials Science Suite 2015-4, was also used for the DFT calculations of ALIE, Fukui functions and BDEs with B3LYP exchange-correlation functional [32], together with 6-311++G(d,p), 6-31++G(d,p) and 6-311G(d,p) basis sets, respectively. For MD simulations Desmond program [33-36], also as implemented in Schrödinger Materials Science Suite 2015-4, was used with OPLS 2005 force field [37] within NPT ensemble class. Simulation time was set to 10 ns, while the whole system was modeled by placing one MPATB molecule in the cubic box with ~3000 water molecule. Other parameters include cut off radius set to 12 Å, temperature to 300 K and pressure to 1.0325 bar. Solvent was treated within simple point charge (SPC) model [38]. Noncovalent interactions were determined by using the method of Johnson [39, 40], as implemented in Jaguar 9.0 program. In all cases

when Jaguar and Desmond were used, input and output files were manipulated by Maestro graphical user interface application for Schrödinger Materials Science Suite 2015-4.

4. Results and discussion

In the following discussions, the rings, C_{41}-C_{43}-C_{47}-C_{45}-C_{42}-C_{40}, C_{29}-C_{27}-C_{25}-C_{26}-C_{28}-C_{31}, N_{35}-C_{24}-O_{34}-C_{25}-C_{26} and C_1-C_2-C_3-C_4-C_5-C_6 are designated as PhI, PhII, PhIII and PhIV, respectively.

4.1 Geometrical parameters

For the title compound, the bond lengths in the phenyl rings are in the range 1.4002-1.3929 Å for PhI, 1.4140-1.3829 Å for PhII and 1.4062-1.3929 Å for PhIV which are in agreement with that of literature [41]. The C_{38}=O_{39} bond length of the title compound is 1.2188 Å which is in agreement with literature [42]. The bond lengths, C_{25}-O_{34} = 1.3711 Å, C_{24}-O_{34} =1.3807 Å, C_{24}=N_{35} = 1.2975 Å, C_{38}-N_{36} = 1.3695 Å, C_{31}-N_{36} =1.4138 Å and C_{26}-N_{35} = 1.3912 Å are different which is due to different environment in the molecular system and C_{24}-N_{35} assumes a double bond character as reported in literature [41].

The bond angles around, C_{47} is C_{45}-C_{47}-C_{43} = 117.8°, C_{45}-C_{47}-C_{53} = 121.1°, C_{43}-C_{47}-C_{53} = 121.1° and this asymmetry in angles is due to interaction between phenyl ring PhI and $H_{48,\,49}$. Similarly at C_{40} position, the angles are, C_{41}-C_{40}-C_{42} = 117.8°, C_{42}-C_{40}-C_{50} = 121.1° and C_{41}-C_{40}-C_{50} = 121.1° which is due to the repulsion between the CH_2 and $H_{44,46}$ of PhI. At C_{25} and C_{26} positions, C_{26}-C_{25}-C_{27} = 123.1°, C_{26}-C_{25}-O_{34} = 107.7°, C_{27}-C_{25}-O_{34} = 129.1Å and C_{25}-C_{26}-C_{28} = 121.1°, C_{25}-C_{26}-N_{35} = 108.4°, C_{28}-C_{26}-N_{35} = 130.5° and this is due to the interaction between rings PhII and PhIII. The bond angles, C_{50}-C_{38}-N_{36} = 115.5°, C_{50}-C_{38}-O_{39} = 119.9°, N_{36}-C_{38}-O_{39} = 124.6° around C_{38} position gives the interaction is due to the neighboring units CH_2, NH. Similarly, at C_{24}, the angles are O_{34}-C_{24}-N_{35} = 114.7°, O_{34}-C_{24}-C_6 = 117.5° and N_{35}-C_{24}-C_6 = 127.9° and this asymmetry is due to interaction between PhIII and neighboring units. The interaction between NH and PhII is given by the bond angles around N_{36} which are C_{31}-N_{36}-C_{38} = 129.2°, C_{31}-N_{36}-H_{37} = 115.4°, C_{38}-N_{36} – H_{37} = 115.4°. The carbonyl group is tilted from the phenyl ring PhI as is evident from the torsion angles, C_{42}-C_{40}-C_{50}-C_{38} = 89.5°, C_{45}-C_{42}-C_{40}-C_{50} = -178.8°, C_{41}-C_{40}-C_{50}-C_{38} = -89.6°, C_{43}-C_{41}-C_{40}-C_{50} = 178.8°.

4.2 IR and Raman spectra

The observed IR, Raman bands, calculated scaled wave numbers and assignments are given in Table 2.

According to literature [43, 44], the NH vibrations are expected in the following regions: stretching mode: 3500-3300 cm^{-1}; deformation modes: around 1500, 1250 and 750-600 cm^{-1}. For the title compound, the NH stretching modes are assigned at 3440 cm^{-1} in the IR spectrum, 3449 cm^{-1} in the Raman spectrum and at 3453 cm^{-1} theoretically and the NH deformations are assigned at 1507, 1263, 646 cm^{-1} theoretically and experimentally bands are observed at 1498, 644 cm^{-1} in the Raman spectrum and 644 cm^{-1} in the IR spectrum. The NH stretching mode has a PED of 100% with IR intensity 108.48 and Raman activity 440.07. The PED of the NH deformation modes are in between 40 and 50%. For the mode at 646 cm^{-1}, the IR intensity and Raman activity are very low, less than 10. The reported values of NH modes are at 3462 cm^{-1} in the IR spectrum, 3450 cm^{-1} in the Raman spectrum, 3400 cm^{-1} theoretically (stretching modes), 1508, 1219, 655 cm^{-1} (DFT) (deformation modes) [42] and 1587, 1250, 650 cm^{-1} (IR), 1580, 1227, 652 cm^{-1} (DFT) (deformation modes) [45].

The C=N stretching mode of the title compound is assigned at 1521 cm^{-1} in the IR spectrum, 1519 cm^{-1} in the Raman spectrum and at 1522 cm^{-1} theoretically as expected [46, 47]. The C-N stretching modes of the title compound are observed at 1192, 1115 cm^{-1} in the IR spectrum, 1242, 1189 cm^{-1} in the Raman spectrum and at 1244, 1189, 1118 cm^{-1} theoretically which are expected in the range 1300-1100 cm^{-1} [47]. All the CN stretching modes have PEDs from 36 to 42% and for the modes, 1522, 1244 cm^{-1} the Raman activity is very high and bands are seen the Raman spectrum.

In the present case, the C=O stretching mode is observed at 1677 cm^{-1} in the IR spectrum, 1670 cm^{-1} in the Raman spectrum, 1674 cm^{-1} theoretically while the C-O stretching modes are assigned at 905 cm^{-1} in the Raman spectrum and at 1174, 903 cm^{-1} theoretically. For the modes, 1674 and 903 cm^{-1} the Raman activities are high, 64.43 and 181.17 and experimentally bands are observed in the Raman spectrum and the PEDs are 74 and 39%. Also the mode at 1674 cm^{-1} has a high IR intensity of 334.39 and a PED of 74%. According to literature, the C=O stretching modes are expected in the region 1850-1550 cm^{-1} [48] and the C-O-C stretching modes are in the region 1200-900 cm^{-1} [47, 49].

Sebastian et al reported the carbonyl stretching mode at 1694 cm^{-1} in the IR spectrum, 1696 cm^{-1} in the Raman spectrum and at 1699 cm^{-1} theoretically [42]. For a benzoxazole derivative, the C-O-C stretching modes are reported at 1173, 890 cm^{-1} in the IR spectrum, 1174, 888 cm^{-1} in the Raman spectrum, 1172, 893 cm^{-1} theoretically by Parveen et al. [41].

The methyl stretching modes of the title compound are observed at 2960, 2903 cm^{-1} in the IR spectrum and at 2983, 2955, 2914 cm^{-1} in the Raman spectrum as expected [43, 46]. The bending modes of the methyl groups are observed at 1427, 1361, 1342, 1018, 984 cm^{-1} in the IR spectrum and at 1461, 1433, 1359, 1338, 1002, 969, 905 cm^{-1} in the Raman spectrum. The DFT calculations give these modes in the ranges 2984- 2904 cm^{-1} (stretching) and 1463-901 cm^{-1} (deformation modes) [43, 46]. The CH_2 modes of the title compound are observed at 1410, 1149 cm^{-1} in the IR spectrum, 1276, 1156 cm^{-1} in the Raman spectrum experimentally and the PED analysis gives these modes at 2968, 2933 cm^{-1} (stretching) and 1408, 1276, 1159, 893 cm^{-1} (deformation modes) which are in agreement with the literature [43, 468].

The CC_3 stretching modes are expected in the ranges 1295-1175 cm^{-1} and 890-710 cm^{-1} [46] and in the present case, these modes are assigned at 1235, 809 cm^{-1} in the IR spectrum, 812 cm^{-1} in the Raman spectrum and at 1234, 1176, 811 cm^{-1} theoretically with PEDs 47, 48 and 52%. For the mode 1234 cm^{-1} the IR intensity is 40.31 and for the other two modes the IR intensity is less than 10.00. Joseph et al. reported the CC_3 stretching modes at 1244, 907 cm^{-1} in the IR spectrum, 1247 cm^{-1} in Raman spectrum and at 1286, 1249, 906 cm^{-1} theoretically [50]. The deformation modes of the CC_3 group are expected in the regions, 435± 85, 335 ± 80 and 300 ± 80 cm^{-1} (total five modes, two asymmetric, one symmetric and two rocking) and for the title compound, these deformation modes are assigned at 446, 384, 374, 342, 284 cm^{-1} theoretically with PEDs, 62, 35, 38, 43, 33% and the IR intensity and Raman activity values are less than 10% and the reported values are 496, 326, 313, 290, 219 cm^{-1} theoretically [50].

The phenyl CH stretching modes are observed at 3020 cm^{-1} in the Raman spectrum for PhI, 3078 cm^{-1} in the IR spectrum, 3121 cm^{-1} in the Raman spectrum for PhII and 3052 cm^{-1} in the IR spectrum, 3085, 3053 cm^{-1} in the Raman spectrum for PhIV [46]. Theoretically these CH stretching modes are assigned in the ranges, 3049-3031 cm^{-1}

for PhI, 3124-3041 cm^{-1} for PhII and 3083-3052 cm^{-1} for PhIV as expected [46]. The phenyl ring stretching modes are assigned in the ranges 1589-1296 cm^{-1} for PhI, 1595-1320 cm^{-1} for PhII and 1586-1280 cm^{-1} for PhIV while experimentally bands are observed at 1578, 1545, 1521, 1279 cm^{-1} in the IR spectrum and at 1610, 1580, 1551, 1519, 1397, 1322 cm^{-1} in the Raman spectrum [46].

Trisubstituted phenyl rings have three frequency intervals for the ring breathing mode: 500-660, 1050-1100 and 600-750 cm^{-1} for light substituent, heavy substituent and mixed substituent according to literature [51]. For the title compound, the ring breathing mode of tri-substituted benzene ring is assigned at 1100 cm^{-1} theoretically. with a PED 04 44% and the IR intensity and Raman activity values are low. The ring breathing mode of tri-substituted phenyl rings are reported at 1110, 1129 cm^{-1} [52] and at 1109 cm^{-1} in the IR spectrum, 1100 cm^{-1} theoretically 1109 cm^{-1} (IR), 1100 cm^{-1} (DFT) [53]. The ring breathing mode of para-substituted phenyl rings with entirely different substituent are expected in the range 780-880 cm^{-1} according to literature [51] and in the present case, this is confirmed by the bands at 824 cm^{-1} and 783 cm^{-1} by PED analysis with PEDs 42 and 48%. For the mode at 783 cm^{-1} the IR intensity is less than 10%. The phenyl ring breathing mode of para substituted phenyl rings was reported at 795 cm^{-1} [54], at 873 cm^{-1} in the IR spectrum and at 861 cm^{-1} theoretically [55] and at 753 cm^{-1} in IR spectrum, 793, 759 cm^{-1} theoretically [56].

The in-plane CH bending modes of the phenyl rings are assigned as 1018 cm^{-1} (IR), 1277, 1188, 1162, 1020 cm^{-1} (DFT) for PhI, 1106 cm^{-1} (Raman), 1236, 1103, 1094 cm^{-1} (DFT) for PhII and 1002 cm^{-1} (Raman), 1293, 1174, 1161, 1000 cm^{-1} (DFT) for PhIV as expected [46]. The out-of-plane CH bending modes of the phenyl rings are assigned at 928 cm^{-1} (IR), 928 cm^{-1} (Raman), 947, 930, 822, 797 cm^{-1} (DFT) for PhI, 875 cm^{-1} (IR), 880 cm^{-1} (Raman), 895, 880, 773 cm^{-1} (DFT) for PhII and at 956 cm^{-1} (IR), 959, 841, 829, 818 cm^{-1} (DFT) for PhIV [46].

4.3 NMR spectra

GIAO ^{1}H and ^{13}C NMR chemical shifts with respect to trimethylsilane were calculated (Table S2-supporting material) using the B3LYP/6-311++G(d,p). The predicted chemical shifts of aromatic protons of the title compound are in the range 7.7001-7.7117 for PhI, 6.2699-9.5267 for PhII and 7.7705-8.9744 for PhIV while the

experimental protons shifts are 7.60-8.11 for PhI, 7.52-8.09 for PhII and 7.11-7.24 for PhIV. For the tert-butyl group, the proton shifts are in the range, 1.6036-2.1832 (calculated), 1.31 (experimental) while in the methyl group, the chemical shift is in the range 2.6774-3.0564 (calculated), 2.26 (experimental) and in methylene group the shifts are 4.0823, 4.0833 (calculated), 7.61 (experimental). The hydrogen atom of amide group in this compound appears at a higher chemical shift of 10.30 experimentally and 6.0895 ppm theoretically. We noted that, δ_{calc} of the NH protons strongly deviate from the experimental data due to the high polarity of these bonds. The range for ^{13}C NMR chemical shift of the typical organic molecule usually is greater than 100 ppm [57] the accuracy ensures reliable interpretation of spectroscopic parameters. The carbon atom of the carbonyl group has a low lying excited state involving the movement of electrons from the oxygen lone pair to anti-bonding π orbital which generates a paramagnetic current [58]. This n→π* transition produces a large shift to a higher wave number, and hence the carbonyl carbon signals have a weaker intensity and appear in the range, 150-220 ppm [59, 60]. Thus it is easy to recognize the carbonyl absorptions from the other resonances and for the title compound carbonyl shift is 162.9137. The aromatic carbons give resonance in overlapped areas of NMR spectrum with chemical shift values from 100 to 150 ppm [61] and in the present case, the chemical shifts of the aromatic carbon atoms are, 129.9396-132.4818 for PhI, 109.535-146.2932 for PhII and 124.8705-152.1844 for PhIV. The chemical shifts of the other carbon atoms are 28.4974 (C53), 43.6937 (C11), 38.7895 (C13), 35.071 (C14), 38.785 (C12) and 51.8989 (C50).

4.4 Frontier Molecular analysis

Using frontier molecular orbital analysis characterization of intra molecular charge transfer through conjugated paths can be explained through the donor – acceptor groups [62]. In the present case the HOMO and LUMO energies are -8.136 and -5.272 eV, respectively. The ionization energy $I = -E_{HOMO} = 8.136$eV and electron affinity $A = -E_{LUMO} = 5.272$eV and energy gap = 2.864 eV. The global chemical descriptors are given as hardness $\eta = (I-A)/2$, chemical potential $\mu = -(I+A)/2$ and electronegativity index $\omega = \mu^2/2\eta$ [63, 64]. In the present case η, μ and ω are 1.432, -6.704 and 15.693 respectively. In the HOMO-LUMO plot (Fig. S3-supporting material), the HOMO is localized over the acetamido group, benzoxazole, trisubstituted phenyl ring and the phenyl ring attached

with the tert-butyl group, while the LUMO is over the tertbutyl phenyl ring, tert-butyl group, benzoxazole ring and trisubstituted phenyl ring. This shows the charge transfer in the molecular system through the conjugated paths.

4.5 Molecular Electrostatic Potential Map

MEP is used for predicting sites in studies of biological recognition and hydrogen bonding interactions and relative reactivity's towards electrophilic attack [65]. Using the B3LYP/6-311++G(d,p) method the reactive sites for electrophilic and nucleophilic attack for the title compound is calculated and shown in Fig. S4 (supporting material).The different values of the electrostatic potential are represented by different colors and increases in the order red < orange < yellow < green < blue. Red indicates the strongest repulsion while blue represents the strongest attraction. From the MEP plot it is clear that the carbonyl group and nitrogen atom in the benzoxazole moiety are the strongest repulsion regions and NH group is the strongest attraction centers.

4.6 ALIE surfaces, non-covalent interactions and Fukui functions

Sites of molecule that are possibly prone to electrophilic attacks are characterized by the lowest values of energy necessary for the removal of electrons. In this work these sites were effectively determined by calculations of average local ionization energy (ALIE), as introduced by Sjoberg et al. [66, 67]. This important quantum-molecular descriptor is defined as a sum of orbital energies weighted by the orbital densities:

$$I(r)=\sum_i \frac{\rho_i(\vec{r})|\varepsilon_i|}{\rho(\vec{r})}, \quad (1)$$

where $\rho_i(\vec{r})$ represents the electronic density of the *i*-th molecular orbital at the point $\vec{r}$, ε_i represents the orbital energy and $\rho(\vec{r})$ is the total electronic density function. Visualization of ALIE results is the most effective if the corresponding ALIE values are mapped to the electron density surface, which is the case in this work, Fig.2.

ALIE surface of MPATB molecule indicate that areas with the lowest ALIE values are located within the all three benzene rings. Beside benzene rings there is one more location where ALIE value is the lowest and that is the near vicinity of nitrogen atom N35, where ALIE has the value of ~199 kcal/mol. On the other side the highest ALIE value for the MPATB molecule was calculated to be ~333 kcal/mol and it is mostly

located in the near vicinity of hydrogen atoms. Analysis of intra-molecular non-covalent interactions revealed only one such interaction, involving oxygen atom O39 and hydrogen atom H32.

Other possibly important molecule locations of the MPATB molecule in this work have been detected employing the concept of Fukui functions. These functions show how electron density changes with the addition or removal of charge. In this way one practically obtains response properties in terms of electron density when molecule acts as electrophile or nucleophile. In Jaguar program the values of Fukui f^+ and f^- functions are calculated in finite difference approximation according to the following equations:

$$f^+ = \frac{\left(\rho^{N+\delta}(r) - \rho^N(r)\right)}{\delta}, \tag{2}$$

$$f^- = \frac{\left(\rho^{N-\delta}(r) - \rho^N(r)\right)}{\delta}, \tag{3}$$

where N represents the number of electrons in reference state of the molecule, while δ is fraction of electron which default value is set to be 0.01 [68]. Same as in the case of ALIE values, values of Fukui functions have been mapped to the electron density surface, Fig.3.

In Fig.3 purple colour has been used as positive one, while the red colour is used as negative one. In the case of Fukui f^+ function purple colour indicates molecule areas where electron density increase with the addition of charge while in the case of Fukui f^- function red colour indicates molecule areas where electron density decreases with the charge removal. Both Fukui functions confirm the importance of benzene rings in terms of reactivity. Namely, purple colour in case of Fukui f^+ function is located in the benzene ring in the vicinity of three methyl groups, while red colour in the case of Fukui f^- function is located again within the benzene ring, this time the one with only one methyl group.

4.7 Nonlinear Optical properties

The polarizability, first and second hyperpolarzabilities of the title compound are respectively, 5.4051×10^{-23}, 1.328×10^{-30} and -603.64×0^{-37} esu. The reported value of a similar derivative is 1.37×10^{-30} esu [69] and in the present case the first hyperpolarizability of the title compound is 10.22 times that of the standard NLO

material urea [70]. The hyperpolarizability values can give information about the physical properties of materials to gain knowledge about the third harmonic signals in molecular systems [71-73]. From the values of hyperpolarizabilities of the title compound, we can conclude that the title compound and its derivatives are good objects for further research in nonlinear optical analysis.

4.8 Natural Bond Orbital Analysis

NBO 3.1 program [74] as implemented in the Gaussian09 package is used for the NBO calculations of the title compound in order to understand various second-order interactions and the important interactions are given in tables S3 and S4 (supporting materials). The strong inter molecular hyper-conjugative interactions are: C_{24}-N_{35} from O_{34} of $n_2(O_{34})\rightarrow\pi^*(C_{24}$-$N_{35})$ with electron density, 0.30911e and stabilization energy 34.08 kJ/mol; C_{24}-O_{34} from N_{35} of $n_1(N_{35})\rightarrow\sigma^*(C_{24}$-$O_{34})$ with electron density 0.06285e and stabilization energy 14.40 kJ/mol; C_{38}-O_{39} from N_{36} of $n_1(N_{36})\rightarrow\pi^*(C_{38}$-$O_{39})$ with electron density 0.28747e and stabilization energy 63.34 kJ/mol; N_{36}-C_{38} from O_{39} of $n_2(O_{39})\rightarrow\sigma^*$ (N_{36}-C_{38}) with electron density 0.0768e and stabilization energy 26.20 kJ/mol. The different bonding in the molecular system are: $n_2(O_{34})$ and n_2 (O_{39}) with higher orbital energies, -0.3291 and -0.23508a.u), considerable p-characters, 100 and 99.97%, low occupation number 1.973332 and 1.85687. While the orbital, $n_1(O_{34})$ and $n_1(O_{39})$ occupy lower energies, -0.58285 and -0.66097a.u with p-characters, 62.30 and 42.05% and high occupation numbers, 1.96958 and 1.97442.Thus, a very close to pure p-type lone pair orbital participates in the electron donation to the $\pi^*(C_{24}$-$N_{35})$ orbital for n_2 $(O_{34})\rightarrow\pi^*(C_{24}$-$N_{35})$, σ^* $(C_{24}$-$O_{34})$ orbital for n_1 $(N_{35})\rightarrow\sigma^*$ $(C_{24}$-$O_{34})$, $\pi^*(C_{38}$-$O_{39})$orbital for n_1 $(N_{36})\rightarrow\pi^*(C_{38}$-$O_{39})$ and$\sigma^*(N_{36}$-$C_{38})$ orbital for n_2 $(O_{39})\rightarrow\sigma^*$ $(N_{36}$-$C_{38})$interaction in the compound.

4.9 Reactive and degradation properties based on autoxidation and hydrolysis

Molecular modeling provides important results thanks to which forced degradation experiments can be significantly rationalized and optimized [75]. Namely, there is clear correlation between the mechanism of autoxidation and BDE for hydrogen abstraction. Concretely, if the BDE for hydrogen abstraction is in the proper interval then particular molecule location can be considered as possible starting point for the mechanism of autoxidation. Concerning the proper interval of BDE values it is important

to know that all peroxy radicals have similar BDE values (87-92 kcal/mol) which can be considered as independent of the chemical surrounding [76, 77]. This implies that if the BDE for hydrogen abstraction at some location is in this interval it can be considered that autoxidation mechanism is possible. However, the study of Wright et al. [78] have shown that autoxidation mechanism is the most probable for molecule where BDE for hydrogen atom is in the interval between 75 and 85 kcal/mol. Beside calculations of BDE for hydrogen abstraction it is also useful to calculate BDE values for the remaining single acyclic bonds since these indicate the weakest bonds, and thus the locations where degradation could start. BDE values for all single acyclic bonds are presented in Fig.4.

Results presented in Fig.4 indicate that it is not likely for MPATB molecule to be prone to autoxidation mechanism since all calculated BDE values for hydrogen abstraction are higher than 92 kcal/mol, although there are two bonds (denoted with 10 and 11) with BDE values close to 92 kca/mol. This further indicates that MPATB molecule is stable in the open air and in the presence of oxygen. Of the remaining single acyclic bonds there are two with the lowest BDE values, around 70 kcal/mol each. Those bonds are denoted with numbers 14 and 17 and they could be the locations where degradation could start.

In order to investigate which atoms of MPATB molecule have pronounced interactions with water molecules, we have calculated RDF as obtained after MD simulations. RDF, g(r), gives the probability of finding a particle in the distance *r* from another particle [79]. In Fig.5 RDFs of atoms with significant interactions with water molecules have been presented. According to the calculated RDFs there are five carbon atoms and four non-carbon atoms with significant interactions with water molecules. Carbon atoms with significant interactions with water molecules are C1, C5, C11, C47 and C53. Of these five, three of them, C1, C5 and C53 have lower peak distances (between 3.5 Å and 4 Å), than atoms C11 and C47 (that have peak distances between 4.5 Å and 5.0 Å). On the other side two carbon atoms with the highest g(r) values are carbon atoms C11 and C53. The fact that carbon atoms C47 and C53 have pronounced interactions with water molecules is very important because the BDE value for the abstraction of nearby hydrogen atom is close to 92 kcal/mol. This further indicates that autoxidation mechanism for MPATB molecule is hard to be expected since oxidation and

hydrolysis could compete at the mentioned molecule location. Concerning the non-carbon atoms the most important RDF is calculated for hydrogen atom H37, for which the highest g(r) value is somewhat higher than 0.9, while the peak distance is located at below 2 Å. Other atoms with significant interactions with water include hydrogen atom H7, nitrogen atom N35 and oxygen atom O39. Oxygen atom O39 has the highest g(r) value of almost 1.0, while its peak distance is located at around 2.7 Å. The importance of nitrogen atom N35 lies in the fact that this atom is also recognized as important reactive center according to the ALIE results.

4.10 Molecular docking studies

Based on the structure of a compound, PASS (Prediction of Activity Spectra) [80] is an online tool which predicts different types of activities. PASS analysis of the title compound predicts activities given in the Table S5 (supporting material), thymidylate synthase activity with probability to be active (Pa) value of 0.754. Thymidylate synthase (TS) is a key enzyme in the synthesis of 2'-deoxythymidine-5'-monophosphate, an essential precursor for DNA biosynthesis. For this reason, this enzyme is a critical target in cancer chemotherapy [81, 82]. Benzoxazole derivatives are used as antitumor activities against human breast cancer cell lines [83, 84]. Thus we choose thymidylate synthase and used as target for docking study. High resolution crystal structure of thymidylate synthase was downloaded from the RSCB protein data bank website with PDB ID: 3TMS. All molecular docking calculations were performed on Auto Dock-Vina software [85] and as in literature [41, 42]. With the help of Discovery Studio Visualizer 4.0 software the active site which binds well are analysed [86] and the weak non-covalent interactions are given in Fig. 6. Amino acid Trp101 forms two π-sigma, π-π T-shaped, π-alkyl interaction with CH_3 group, phenyl rings respectively. Phe149 forms π-π T-shaped and Tyr164 forms π-stacked interactions with phenyl ring. Ser131 shows H-bond with benzoxazole ring. The docked ligand forms a stable complex with thymidylate synthase (Fig. S5-supporting material) and got a binding affinity value of -8.5kcal/mol (Table 3). These studies show that the title compound can be used for developing new anti-cancerous drug.

5. Conclusion

5-[(4-methylphenyl)acetamido]-2-(4-tertbutylphenyl)benzoxazole was synthesized and characterised by experimental and theoretical methods. The structure, vibrational wave

numbers, NMR, frontier molecular orbital, MEP, NLO and NBO analysis of the title compound is carried out by DFT level using the B3LYP/6-311++G(d,p) basis set. The calculated geometrical parameters were found to be in good agreement with that of similar derivatives. The stability and intermolecular interaction have been interpreted by NBO analysis. ALIE surface recognized benzene rings and nitrogen atom N35 as important reactive centres possibly prone to electrophilic attacks. Fukui functions also indicated the importance of benzene rings from the aspect of reactivity. BDE values for hydrogen abstraction indicate that MPATB molecule is highly stable in the open air and in the presence of oxygen. RDF indicate that five carbon atoms and four non-carbon atoms have significant interactions with water molecule, among which the most important is the hydrogen atom H37. The title compound binds at the active site of the substrate by weak non-covalent interactions and the amino acid Trp101 forms two π-sigma, π-π T-shaped, π-alkyl interaction with CH_3 group, phenyl rings respectively; Phe149 forms π-π T-shaped and Tyr164 forms π-stacked interactions with phenyl ring. Ser131 shows H-bond with benzoxazole ring.

Acknowledgments

The authors would like to extend their appreciation to the Deanship of Scientific Research at KingSaud University for funding this study through the research group project No. RGP-1435-062. The authors are thankful to University of Antwerp for access to the University's CalcUA supercomputer cluster and the support received from Schrödinger Inc.

References

[1] M. Arisoy, O. Temiz-Arpaci, I. Yildiz, F. Kaynak-Onurdag, E. Aki, I. Yalcin, U. Abbasoglu, Synthesis, antimicrobial activity annd QSAR studies of 2,5-disubstituted benzoxazole, SAR and QSAR Environ. Res. 19 (2008) 589-612.

[2] M. Arisoy, O. Temiz-Arpaci, F. Kaynak-Onurdag, S. Ozgen, Novel benzoxazoles, synthesis and antibacterial, antifungal and antitubercular activity against antibiotic resistant and sensitive microbes, Z. Naturforsch. 68C (2013) 453-460.

[3] M. Arisoy, O. Temiz-Arpaci, F. Kaynak-Onurdag, S. Ozgen, Synthesis and antimicrobial activity of novel benzoxazoles, Z. Naturforsch. 67C (2012) 466-472.

[4] O. Temiz-Arpaci, B.E. Cifcioglu-Goztepe, F. Kaynak-Onurdag, S. Ozgen, F.S. Senol, I.Erdogan-Orhan, Synthesis and different biological activitie sof novel benzoxazoles, Acta Biol. Hungarica 64 (2013) 249-261.

[5] M. Arisoy, O. Temiz-Arpaci, F. Kaynak-Onurdag, S. Ozgen, Synthesis and antimicrobial evaluation of 2-(p-substituted phenyl)-5-[(4-substituted piperazin-1-yl)acetamido]-benzoxazoles, Z. Naturforsch. 69C (2014) 368-374.

[6] D.N. Ward, D.C. Talley, M. Tavag, S. Menji, P. Schaughency, A. Baier, P.J. Smith, UK-1 and structural analogs are potent inhibitors of hepatitis C virus replication, Bioorg. Med. Chem. Lett. 24 (2014) 609-612.

[7] J. Vinsova, K. Cermakova, A. Tomeckova, M. Ceckova, J. Jampilek, P.Cemak, J. Kunes, M. Dolezal, F. Staud, Synthesis and antimicrobial evaluation of new 2-substituted 5,7-tert-butylbenzoxazoles, Bioorg. Med. Chem. 14 (2006) 5850-5865.

[8] L. Oehlers, C.L. Mazzitelli, J.S. Brodbelt, M. Rodriguez, S. Kerwin, Evaluation of complexes of DNA duplexes and novel benzoxazoles or benzimidazoles by electrospray ionization mass spectrometry, J. Am. Soc. Mass Spectrom. 15 (2004) 1593-1603.

[9] S. Braun, A. Botzki, S. Salmen, C. Textor, G. Bernhardt, S. Dove, A. Buschauer, Design of benzimidazole and benzoxazole-2-thione derivatives as inhibitors of bacterial hyaluronan lyase, Eur. J. Med. Chem. 46 (2011) 4419-4429.

[10] J. Kozic, E. Novotna, M. Volkova, J. Storlarikova, F. Trejtnar, V. Wsol, J. Vinsova, Synthesis and in vitro antimycobacterial and isocitrate lyase inhibition properties of novel 2-methoxy-2'-hydroxybenzanilides, their thioxo analogues and benzoxazoles, Eur. J. Med. Chem. 56 (2012) 108-119.

[11] M.A. Weidner-Wells, K.A. Ohemeng, V.N. Nguyen, S. Fraga-Spano, M.J. Macielag, H.M. Werblood, B.D. Foleno, G.C. Webb, J.F. Barrett, D.J. Hlasta, Amidino benzimidazole inhibitors of bacterial two component systems, Bioorg. Med. Chem. Lett. 11 (2001) 1545-1548.

[12] D.J. Hlasta, J.P. Demers, B.D. Foleno, S.A. Fraga-Spano, J. Guan, J.J. Hilliard, M.J. Macielag, K.A. Ohemeng, C.M. Sheppard, Z. Sui, G.C. Webb, M.A. Weidner-Wells, H. Werblood, J.F. Barrett, Novel inhibitors of bacterial two

component systems with gram positive antibacterial activity, pharmacophore identification based on the screening hit closantel, Bioorg. Med. Chem. Lett. 8 (1998) 1923-1928.

[13] A.F. Mabied, E.M. Shalaby, H.A. Zayed, E. El-Kholy, I.S. Faraq, N.A. Ahmed, Crystal structure and stereochemistry study of 2-substituted benzoxazole derivatives, ISRN Org. Chem. doi.org/10.1155/2014/728343.

[14] N.D. Jayanna, H.M. Vagdevi, J.C. Dharshan, T.R.P. Kekuda, Synthesis, antibacterial and antioxidant evaluation of novel 1-(5,7-dichloro-1,3-benzoxazol-2-yl)-1H-pyrazolo[3,4-b]quinoline derivatives, J. Chem. doi.org./ 10.1155/ 2013/ 234074.

[15] A. Golubović, B. Abramović, M. Šćepanović, M. Grujić-Brojčin, S. Armaković, I. Veljković, B. Babić, Z. Dohčević-Mitrović, Z. Popović, Improved efficiency of sol-gel synthesized mesoporous anatase nanopowders in photocatalytic degradation of metoprolol, Mater. Res. Bull. 48 (2013) 1363-1371.

[16] R. Ma, B. Wang, S. Lu, Y. Zhang, L. Yin, J. Huang, S. Deng, Y. Wang, G. Yu, Characterization of pharmaceutically active compounds in Dongiting Lake, China: Occurrence, chiral profiling and environmental risk, Sci. Total Environ. 557 (2016) 268-275.

[17] S.J. Armaković, S. Armaković, N.L. Finčur, F. Šibul, D. Vione, J.P. Šetrajčić, B. Abramović, Influence of electron acceptors on the kinetics of metoprolol photocatalytic degradation in TiO_2 suspension: A combined experimental and theoretical study, RSC Advances 5 (2015) 54589-54604.

[18] B. Abramovic, S. Kler, D. Sojic, M. Lausevic, T. Radovic, D. Vione, Photocatalytic degradation of metoprolol tartrate in suspensions of two TiO2-based photocatalysts with different surface area. Identification of intermediates and proposal of degradation pathways, J. Hazard. Mater. 198 (2011) 123-132.

[19] B. Abramovic, S. Kler, D. Sojic, M. Lausevic, T. Radovic, D. Vione, Photocatalytic degradation of metoprolol tartrate in suspensions of two TiO2-based photocatalysts with different surface area. Identification of intermediates and proposal of degradation pathways, J. Hazard. Mater. 198 (2011) 123-132.

[20] J.J. Molnar, J.R. Agbaba, B.D. Dalmacija, M.T. Klašnja, M.B. Dalmacija, M.M. Kragulj, A comparitive study of the effects of ozonation and TiO_2 catalzed ozonation on the selected chlorine disinfection by product precursor content and structure, Sci. Total Environ. 425 (2012) 169-175.

[21] J. Molnar, J. Agbaba, B. Dalmacija, M. Klašnja, M. Watson, M. Kragulj, Effects of ozonation and catalytic ozonation on the removal of natural organic matter from groundwater, J. Environ. Engineering 138 (2011) 804-808.

[22] M. Blessy, R.D. Patel, P.N. Prajapati, Y. Agrawal, Development of forced degradation and stability indicating studies of drugs, a review, J. Pharm. Anal. 4 (2014) 159-165.

[23] CLSI (2006), Reference method for broth dilution antifungal susceptibility testing yeast; approved standard, M27-A3. Clinical and Laboratory Standards Institute, Wayne, PA, USA.

[24] CLSI (2008), Performance standards for antimicrobial susceptibility testing; 16th informational supplement, CLSI M100-S18. Clinical and Laboratory Standards Institute, Wayne, PA, USA.

[25] A.D. Becke, Density functional exchange energy approximation with correct asymptotic behavior, Phys. Rev. A38 (1988) 3098-3100.

[26] C. Lee, W. Yang, R.G. Parr, Development of the Colle-Salvetti correlation energy formula into a functional of the electron density, Phys. Rev. B 37 (1988) 785-789.

[27] Gaussian 09, Revision C.01, M.J. Frisch, G.W. Trucks, H.B. Schlegel, G.E. Scuseria, M.A. Robb, J.R. Cheeseman, G. Scalmani, V. Barone, B. Mennucci, G.A. Petersson, H. Nakatsuji, M. Caricato, X. Li, H.P. Hratchian, A.F. Izmaylov, J. Bloino, G. Zheng, J.L. Sonnenberg, M. Hada, M. Ehara, K. Toyota, R. Fukuda, J. Hasegawa, M. Ishida, T. Nakajima, Y. Honda, O. Kitao, H. Nakai, T. Vreven, J.A. Montgomery, Jr., J.E. Peralta, F. Ogliaro, M. Bearpark, J.J. Heyd, E. Brothers, K.N. Kudin, V.N. Staroverov, T. Keith, R. Kobayashi, J. Normand, K. Raghavachari, A. Rendell, J.C. Burant, S.S. Iyengar, J. Tomasi, M. Cossi, N. Rega, J.M. Millam, M. Klene, J.E. Knox, J.B. Cross, V. Bakken, C. Adamo, J. Jaramillo, R. Gomperts, R.E. Stratmann, O. Yazyev, A.J. Austin, R. Cammi, C.

Pomelli, J.W. Ochterski, R.L. Martin, K. Morokuma, V.G. Zakrzewski, G.A. Voth, P. Salvador, J.J. Dannenberg, S. Dapprich, A.D. Daniels, O. Farkas, J.B. Foresman, J.V. Ortiz, J. Cioslowski, D.J. Fox, Gaussian, Inc., Wallingford CT, 2010.

[28] J.B. Foresman, P.A. Pittsburg in: E. Frisch (Ed.), Exploring Chemistry with Electronic Structure Methods: a Guide to Using Gaussian, 1996.

[29] J.M.L. Martin, C. Van Alsenoy, GAR2PED, a Program to Obtain a Potential Energy Distribution from a Gaussian Archive Record, University of Antwerp, Belgium, 2007.

[30] R. Dennington, T. Keith, J. Millam, Gaussview, Version 5, Semichem. Inc., ShawneeMission, KS, 2009.

[31] *Schrödinger Materials Science User Manual*. 2014, Schrödinger Press.

[32] A.D. Becke, Density functional thermochemistry. III. The role of exact exchange, J. Chem. Phys. 98 (1993) 5648-5652.

[33] D. Shivakumar, J. Williams, Y. Wu, W. Damm, J. Shelley, W. Sherman, Prediction of absolute solvation free energies using molecular dynamics free energy perturbation and the OPLS force field, J. Chem. Theory Comput. 6 (2010) 1509-1519.

[34] Z. Guo, U. Mohanty, J. Noehre, T.K. Sawyer, W. Sherman, G. Krilov, Probing the α-helical structural stability of stapled p53 peptides: Molecular dynamics simulations and anlaysis, Chem. Biol. Drug Design 75 (2010) 348-359.

[35] K.J. Bowers, E. Chow, H. Xu, R.O. Dror, M.P. Eastwood, B.A. Gregersen, J.L. Klepeis, I. Kolossvary, M.A. Moraes, F.D. Sacerdoti, *Scalable algorithms for molecular dynamics simulations on commodity clusters*. in *SC 2006 Conference, Proceedings of the ACM/IEEE*. 2006. IEEE.

[36] *Schrödinger Release 2015-4: Desmond Molecular Dynamics System, version 4.4, D. E. Shaw Research, New York, NY, 2015. Maestro-Desmond Interoperability Tools, version 4.4, Schrödinger, New York, NY, 2015*. 2015.

[37] J.L. Banks, H.S. Beard, Y. Cao, A.E. Cho, W. Damm, R. Farid, A.K. Felts, T.A. Halgren, D.T. Mainz, J.R. Maple, R. Murphy, DM. Philipp, M.P. Repasky, L.Y. Zhang, B.J. Berne, R.A. Friesner, E. Gallicchio, R.M. Lew, Integrated modeling

program, applied chemical theory (IMPACT), J. Comput. Chem. 26 (2005) 1752-1780.

[38] H.J. Berendsen, J.P. Postma, W.F. van Gunsteren, J. Hermans, *Interaction models for water in relation to protein hydration*, in *Intermolecular forces*. 1981, Springer. p. 331-342.

[39] A. Otero-de-la-Roza, E.R. Johnson, J. Contreras-García, Revealing non-covalent interactions in solids: NCI plots revisited, Phys. Chem. Chem. Phys. 14 (2012) 12165-12172.

[40] E.R. Johnson, S. Keinan, P. Mori-Sanchez, J. Contreras-Garcia, A.J. Cohen, W. Yang, Revealing nonocovalent interactions, J. Am. Chem. Soc. 132 (2010) 6498-6506.

[41] S.S. Parveen, M.A. Al-Alshaikh, C.Y. Panicker, A.A. El-Emam, M. Arisoy, O. Temiz-Arpaci, C. Van Alsenoy, Synthesis, vibrational spectroscopic investigations, molecular docking, antibacterial and antimicrobial studies of 5-ethylsulphonyl-2-(p-aminophenyl)benzoxazole, J. Mol. Struct. 1115 (2016) 94-104.

[42] S.H.R. Sebastian, M.A. Al-Alshaikh, A.A. El-Emam, C.Y. Panicker, J. Zitko, M. Dolezal, C. Van Alsenoy, Spectroscopic, quantum chemical sttudies, Fukui functions, in vitro antiviral activity and molecular docking of 5-chloro-N-(3-nitrophenyl)pyrazine-2-carboxamide, J. Mol. Struct. 1119 (2016) 188-199.

[43] N.B. Colthup, L.H. Daly, S.E.Wiberly, Introduction of Infrared and Raman Spectroscopy, Academic Press, New York, 1975.

[44] L.J. Bellamy, The Infrared Spectrum of Complex Molecules, third Edn., Chapman and Halls, London, 1975.

[45] Y.S. Mary, H.T. Varghese, C.Y. Panicker, M. Dolezal, Vibrational spectroscopic studies and ab initio calculations of a substituted amide of pyrazine-2carboxylic acid – $C_{12}H_{10}ClN_3O$, Spectrochim. Acta A 71 (2008) 725-730.

[46] N.P.G. Roeges, A Guide to the Complete Interpretation of Infrared Spectra of Organic Structures, John Wiley and Sons, New York, 1994.

[47] R.M. Silverstein, G.C. Bassler, T.C. Morril, Spectrometric Identification of Organic Compounds, fifth ed., John Wiley and Sons Inc., Singapore, 1991.

[48] G. Socrates, Infrared Characteristic Group Frequencies, John Wiley and Sons, New York, 1981.

[49] J.B. Bhagyasree, J. Samuel, H.T. Varghese, C.Y. Panicker, M. Arisoy, O. Temiz-Arpaci, Synthesis, FT-IR investigations and computational study of 5-[(4-bromophenyl)acetamido]2-(4-tert-butylphenyl)benzoxazole, Spectrochim. Acta A 115 (2013) 79-91.

[50] T. Joseph, H.T. Varghese, C.Y. Panicker, K. Viswanathan, M. Dolezal, T.K. Manojkumar, C. Van Alsenoy, Vibrational spectroscopic investigations and computational study of 5-tert-butyl-N-(4-trifluoromethylphenyl)pyrazine-2-carboxamide, Spectrochim. Acta A 113 (2013) 203-214.

[51] G. Varsanyi, Assignments of Vibrational Spectra of Seven Hundred Benzene Derivatives, Wiley, New York, 1974.

[52] V.S. Madhavan, H.T. Varghese, S. Mathew, J. Vinsova, C.Y. Panicker, FT-IR, FT-Raman and DFT calculations of 4-chloro-2-(3,4-dichlorophenylcarbamoyl) phenyl acetate, Spectrochim. Acta A 72 (2009) 547-553.

[53] S.H.R. Sebastian, A.M.S. Al-Tamimi, N.R. El-Brollosy, A.A. El-Emam, C.Y. Panicker, C. Van Alsenoy, Vibrational spectroscopic (FT-IR and FT-Raman) studies, HOMO-LUMO, NBO analysis and MEP of 6-methyl-1-({[(2E)-2-methyl-3-phenyl-prop-2-en-1-yl]oxy}methyl)-1,2,3,4-tetra-hydroquinazoline-2,4-dione, a potential chemotherapeutic agent, using density functional methods, Spectrochim. Acta A 134 (2015) 316-325.

[54] Y.S. Mary, C.Y. Panicker, M. Sapnakumari, B. Narayana, B.K. Sarojini, A.A. Al-Saadi, C. Van Alsenoy, J.A. War, FT-IR, FT-Raman, HOMO-LUMO, MEP analysis and molecular docking study of 1-[3-(4-fluorophenyl)-5-phenyl-4,5-dihydro-1H-pyrazol-1-yl]ethanone, Spectrochim. Acta A 136 (2015) 483-493.

[55] C.Y. Panicker, K.R. Ambujakshan, H.T. Varghese, S. Mathew, S. Ganguli, A.K. Nanda, C. Van Alsenoy, FT-IR, FT-Raman and DFT calculations of 3-{[(4-fluorophenyl)methylene]amino}-2-phenlquinazolin-4(3H)-one, J. Raman Spectrosc. 40 (2009) 527-536.

[56] Y.S. Mary, C.Y. Panicker, M. Sapnakumari, B. Narayana, B.K. Sarojini, A.A. Al-

Saadi, C. Van Alsenoy, J.A. War, H.K. Fun, Molecular structure, FT-IR, vibrational assignments, HOMO-LUMO analysis and molecular docking study of 1-[5-(4-bromophenyl)3-(4-fluorophenyl)-4,5-dihydro-1H-pyrazol-1-yl]ethanone, Spectrochim. Acta A 136 (2015) 473- 482.

[57] Y. Ataly, D. Avci, A.Basoglu, Linear and nonlinear optical properties of some donor-acceptor oxadizoles by ab initio Hartree-Fock calculations, Struct. Chem. 19 (2008) 239-246.

[58] M. Cinar, M. Karabacak, Determination of conformational and spectroscopic features of ethyl trans-alfa-cyano-3-indole-acrylate compound, an experimental and quantum chemical study, Spectrochim. Acta A 104 (2013) 428-436.

[59] M. Venkatanarayana, P.K. Dubey, L-proline-catalyzed knoevenagel condensation: A facile, green synthesis of (E)-ethyl-2-cyano-3-(1H-indol-3-yl)acrylates and (E)-3-(1H-indol-3-yl)acrylonitriles, Synth. Commun. 42 (2012) 1746-1759.

[60] J.S. Yadav, B.V.S. Reddy, A.K. Basak, B. Visali, A.V. Narsaiah, K. Nagaiah, Phosphane catalyzed knoevenagel condensation: A facile synthesis of α-cyanoacrylonitriles, Eur. J. Org. Chem. (2004) 546-551.

[61] H.O. Kalinowski, S. Berger, S. Braun, Carbon-13 NMR Spectroscopy, John Wiley and Sons, Chichester, 1988.

[62] B. Kosar, C. Albayrak, Spectroscopic investigations and quantum chemical computational study of (E)-4-methoxy-2-[(p-tolylimino)methyl]phenol, Spectrochim. Acta A 78 (2011) 160-167.

[63] R.J. Parr, L.V. Szentpaly, Electrophilicity index, S. Liu, J. Am. Chem. Soc. 121 (1999) 1922-1924.

[64] R.J. Parr, R.G. Pearson, Absolute hardness, companion parameter to absolute electronegativity , J. Am. Chem. Soc. 105 (1983) 7512-7516.

[65] E. Scrocco, J. Tomasi Reactivity and intermolecular forces, an euristic interpretation by means of electrostatic molecular potentials, Adv. Quantum Chem. 11 (1978) 115-193.

[66] J.S. Murray, J.M. Seminario, P. Politzer, P. Sjoberg, Average local ionization energies computd on the surfaces of some strained molecules, Int. J. Quantum Chem. 38 (1990) 645-653.

[67] P. Politzer, F. Abu-Awwad, J.S. Murray, Comparison of density functional and Haratree-Fock average local ionization energies on molecular surfaces, Int. J. Quantum Chem. 69 (1998) 607-613.

[68] A. Michalak, F. De Proft, P. Geerlings, R. Nalewajski, Fukui functions from the relaxed Kohn-Sham orbitals, J. Phys. Chem. A103 (1999) 762-771.

[69] J.B. Bhagrasree, J. Samuel, H.T. Varghese, C.Y. Panicker, M. Arisoy, O. Temiz-Arpaci, Synthesis, FT-IR investigation and computational study of 5-[(4-bromophenyl)acetamido]-2-(4-tert-butylphenyl)benzoxazole, Spectrochim. Acta A 115 (2013) 79-91.

[70] C. Adant, M. Dupuis, J.L. Bredas, Ab initio study of the nonlinear optical properties of urea, electron correlation and dispersion effects, Int. J. Quantum Chem. 56 (1995) 497-507.

[71] D. Tokarz, R. Cisek, N. Prent, U. Fekl, V. Barzda, Measuring the molecular second hyperpolarizability in absorptive solutions by the third harmonic generation ratio technique, Anal. Chim. Acta 755 (201) 86-92.

[72] R. Cisek, L. Spencer, N. Prent, D. Zigmantas, G. Espie, V. Barzda, Optical microscopy in photosynthesis, Photosynth. Res. 102 (2009) 111-141.

[73] W.J. Nie, Optical nonlinearity, phenomena, applications and materials, Adv. Mater. 5 (1993) 520.

[74] E.D. Glendening, A.E. Reed, J.E. Carpenter, F. Weinhold, NBO Version 3.1.

[76] T. Andersson, A. Broo, E. Evertsson, Prediction of drug candidates sensitivity toward autoxidation: computational estimation of C-H dissociation energies of carbon centered radicals, J. Pharm. Sci. 103 (2014) 1949-1955.

[75] P. Lienard, J. Gavartin, G. Boccardi, M. Meunier, Predicting drug substances autoxidation, Pharm. Res. 32 (2015) 300-310.

[77] Y-R.Luo, *Handbook of bond dissociation energies in organic compounds*. 2002: CRC press.

[78] J.S. Wright, H. Shadnia, L.L. Chepelev, Stability of carbon centered radicals, effect of functional groups on the energetic of addition of molecular oxygen, J. Comput. Chem. 30 (2009) 1016-1026.

[79] R.V. Vaz, J.R. Gomes, C.M. Silva, Molecular dynamics simulation of diffusion coefficients and structural properties of ketones in supercritical CO_2 at infinite dilution, J. Supercritic. Fluids 107 (2016) 630-638.

[80] A. Lagunin, A. Stepanchikova, D. Filimonov, V. Poroikov, PASS: prediction of activity spectra for biologically active substances, Bioinformatics 16 (2000) 747-748.

[81] M.G. Rose, M.P. Farrell, J.C. Schmitz, Thymidylate synthase, a critical target for cancer chemotherapy, Clin. Colorectal. Cancer 1 (2002) 220-229.

[82] Y.M. Rustum, A. Harstrick, S. Cao, U. Vanhoefer, M.B. Yin, H. Wilke, S. Seeber, Thymidylate synthase inhibitors in cancer therapy, direct and indirect inhibitors, J. Clin. Oncol. 15 (1997) 389-400.

[83] M.A. Abdelgawad, A. Belal, H.A. Omar, L. Hegazy, M.E. Rateb, Synthesis, antibreast cancer activity, and molecular modeling of some benzothiazole and benzoxazole derivatives, Arch. Pharm. 346 (2013) 534-541.

[84] A.A. Fadda, E.A. Latif, E.H. Tawfik, R.M. Mohammed, Synthesis of some new benzoxazole derivatives and their cytotoxicity to human cancer cell lines, Res. J. Pharm. Biol. Chem. Sci. 7 (2016) 1820-1826.

[85] O. Trott, A. J. Olson, AutoDock Vina: Improving the speed and accuracy of docking with a new scoring function, effiecient otimization and multithreading, J. Comput. Chem. 31 (2010) 455-461.

[86] B. Kramer, M. Rarey, T. Lengauer, Evaluation of the FlexX incremental construction algorithm for protein ligand docking, PROTEINS: Struct. Funct. Genet. 37 (1999) 228-241.

Figure captions

Fig.1 Optimized geometry of 5-[(4-methylphenyl)acetamido]-2-(4-tert-butylphenyl) benzoxazole

Fig.2 ALIE surface of 5-[(4-methylphenyl)acetamido]-2-(4-tert-butylphenyl) benzoxazole molecule

Fig.3 Fukui functions a) f^+ and b) f^- of 5-[(4-methylphenyl)acetamido]-2-(4-tert-butylphenyl) benzoxazole molecule

Fig.4 BDEs of all single acyclic bonds of 5-[(4-methylphenyl)acetamido]-2-(4-tert-butylphenyl) benzoxazole molecule

Fig.5 RDFs of atoms of 5-[(4-methylphenyl)acetamido]-2-(4-tert-butylphenyl) benzoxazole with pronounced interactions with water: a) carbon atoms and b) non-carbon atoms

Fig.6 Amino acids of thymidylate synthase receptor interaction with the docked ligand and receptor surface as background

Table 1

Antimicrobial and antitubercular activity (MIC μg/ml) of synthesized compound **6** and the standard drugs.

	Microorganisms[a]											
Compound	E.c.	E.c*	K.p.	K.p*	S.a.	S.a*	E.f.	E.f*	C.a	C.k.	M.t.	M.t.*
-	32	64	32	128	128	128	64	128	64	64	8	8
Vancomycin	n.d.[b]	n.d.	n.d.	n.d.	1	1	1	32	n.d.	n.d.	n.d.	n.d.
Gentamycin sulfate	1	1024	0.5	256	0.125	32	4	32	n.d.	n.d.	n.d.	n.d.
Meropenem	0.0625	<0.0625	0.03	<0.0625	0.125	-	2	0.5	n.d.	n.d.	n.d.	n.d.
Ofloxacin	<0.0625	64	0.125	0.5	0.125	0.25	1	4	n.d.	n.d.	n.d.	n.d.
Amipicillin	2	>2048	2	>2048	0.5	>2048	1	0.5	n.d.	n.d.	n.d.	n.d.
AmphotericinB	n.d.	n.d.	n.d.	n.d.	n.d.	n.d.	n.d.	n.d.	0.25	2	n.d.	n.d.
Fluconzaloe	n.d.	n.d.	n.d.	n.d.	n.d.	n.d.	n.d.	n.d.	1	64	n.d.	n.d.
Isoniazid	n.d.	n.d.	n.d.	n.d.	n.d.	n.d.	n.d.	n.d.	n.d.	n.d.	<0.25	<0.25
Ethambutol	n.d.	n.d.	n.d.	n.d.	n.d.	n.d.	n.d.	n.d.	n.d.	n.d.	2	2

[a]E.c., *Escherichia coli* ATCC 25922; E.c.*,*Escherichia coli* isolate (ESBL); K.p., *Klebsiella pneumoniae* RSKK 574; K.p.*, *Klebsiella pneumoniae* isolate (ESBL); S.a.,*Staphylococcus aureus* ATCC 29213; S.a.*, *Staphylococcus aureus* isolate (MRSA); E.f., *Enterococcus faecalis* ATCC 29212; E.f.*: *Enterococcus faecalis* isolate (VRE); C.a.,*Candida albicans* ATCC 10231;C.k., *Candida krusei* ATCC 6258; M.t., *Mycobacterium tuberculosis* H37RV ATCC 27294; M.t.*, *Mycobacterium tuberculosis* isolate.

[b]n.d., not determined (microbiological assays were not performed due to following reasons: antibacterial drugs were not assayed against fungi and *M. tuberculosis*; antifungal drugs were not assayed against bacteria and *M. tuberculosis*; antitubercular drugs were not assayed against bacteria and fungi; Gram-negative bacteria employed in the study are naturally resistant to vancomycin).

Table 2

Calculated scaled wave numbers, observed IR, Raman bands and assignments

B3lYP/6-311++G(d,p)			IR	Raman	Assignments[a]
υ(cm^{-1})	IRI	RA	υ(cm^{-1})	υ(cm^{-1})	-
3453	108.48	440.07	3440	3449	υNH(100)
3124	11.64	33.28	-	3121	υCHII(99)
3083	7.36	130.46	-	3085	υCHIV(98)
3079	3.44	114.66	3078	-	υCHII(96)
3076	3.56	46.77	-	-	υCHIV(98)
3067	3.28	42.63	-	-	υCHIV(99)
3052	14.93	78.39	3052	3053	υCHIV(98)
3049	0.63	276.62	-	-	υCHI(98)
3046	27.77	8.83	-	-	υCHI(99)
3041	8.31	94.94	-	-	υCHII(96)
3031	0.22	110.21	-	3020	υCHI(99)
3031	19.29	3.54	-	3020	υCHI(98)
2984	14.84	58.54	-	2983	υCH_3(100)
2979	43.18	68.68	-	-	υCH_3(95)
2976	18.84	38.16	-	-	υCH_3(91)
2973	110.63	373.72	-	-	υCH_3(96)
2970	21.28	29.22	-	-	υCH_3(86)
2968	3.27	65.74	-	-	υCH_2(100)
2965	6.43	46.42	-	-	υCH_3(95)
2964	3.41	16.43	-	-	υCH_3(96)
2958	15.69	100.35	2960	2955	υCH_3(99)
2933	11.70	224.30	-	-	υCH_2(100)
2912	38.67	608.01	-	2914	υCH_3(100)
2906	32.62	375.49	-	-	υCH_3(99)
2904	26.96	27.42	2903	-	υCH_3(94)
2904	27.86	12.21	2903	-	υCH_3(100)
1674	334.39	64.43	1677	1670	υC=O(74)

1595	2.85	1704.08	-	1610	υPhII(42), υPhI(19)
1589	1.69	91.89	-	-	υPhI(62), δCHI(21)
1586	14.82	2757.26	-	1580	υPhIV(44), υPhII(12)
1580	65.94	136.66	1578	-	υPhII(49), υPhI(23)
1548	93.68	1291.13	1545	1551	υC=N(17), υPhIV(47)
1546	0.27	4.56	-	-	υPhI(70), υC=N(11)
1522	147.17	1936.56	1521	1519	υC=N(41), υPhIV(47)
1507	380.29	193.57	-	1498	δNH(50), υCN(15)
1485	25.12	6.15	-	-	δCHI(22), υPhI(46)
1475	78.87	199.25	1478	-	δCHIV(26), υC=N(19), υPhIV(27)
1463	4.99	0.57	-	1461	δCH_3(86)
1450	8.14	10.13	-	-	δCH_3(91)
1449	369.22	52.20	-	-	υPhII(47), δCHII(18), υCN(15)
1446	8.58	10.04	-	-	δCH_3(88)
1437	11.51	8.04	-	-	δCH_3(86)
1434	2.18	7.88	-	-	δCH_3(88)
1433	7.03	16.15	-	1433	δCH_3(95)
1430	0.10	8.47	-	-	δCH_3(87)
1425	0.01	1.20	1427	-	δCH_3(85)
1408	18.85	68.76	1410	-	δCH_2(84)
1399	8.79	937.74	-	1397	υPhII(43), δCHII(20), υCN(11)
1385	1.14	0.57	-	-	υPhI(46), δCHI(20), δCH_3(10)
1384	21.76	310.36	-	-	υPhIV(49), δNH(17)
1376	4.28	4.25	-	-	δCH_3(95)
1361	0.86	24.06	1361	1359	δCH_3(89)
1344	8.39	20.09	1342	1338	δCH_3(89)
1344	8.37	0.02	1342	1338	δCH_3(95)

1320	33.10	121.11	-	1322	υPhII(65), δCHII(10)
1296	0.15	0.72	-	-	δCHI(22), υPhI(50)
1293	8.57	59.14	-	-	δCHIV(50), υPhIV(15)
1280	1.54	17.75	1279	-	υPhIV(61), δCHIV(13)
1277	0.01	2.37	-	-	υPhI(80)
1276	3.40	48.77	-	1276	δCH_2(65), υCC(12)
1263	3.64	38.52	-	-	υCC(13), δNH(42), υPhIV(10), υPhII(14)
1244	39.93	1886.24	-	1242	υCN(42), υPhII(10), δPhIII(11)
1236	5.03	283.76	-	-	δCHII(53), υPhII(11)
1234	40.31	32.57	1235	-	υCC_3(47), δCH_3(20)
1189	190.69	177.90	1192	1189	υCN(36), υCC(14), δNH(18)
1188	10.62	2.74	-	-	υCC(35), δCHI(49)
1176	5.95	8.53	-	-	υCC_3(48), δCH_3(37)
1174	19.53	8.92	-	-	υCO(39), δCHIV(38)
1174	3.23	12.36	-	-	δCH_3(43), υCO(42)
1173	5.42	78.98	-	-	υCC(30), υPhI(22)
1162	0.51	19.51	-	-	δCHI(78)
1161	91.21	530.43	-	-	υCO(18), δCHIV(40), δCHII(12)
1159	0.07	21.5	1149	1156	δCH_2(65), υPhI(16)
1118	11.14	43.38	1135	-	υCN(41), δCHII(19)
1103	4.40	25.67	-	1106	δCHII(57), υPhII(12)
1100	5.59	3.85	-	-	δCHIV(26), υPhII(44)
1094	7.26	0.22	-	-	δCHII(46), υPhI(30)
1085	32.00	124.94	-	1088	υPhIV(31), δCH_3(52)
1027	34.79	46.95	-	1028	υPhIV(24), υCC(35)
1020	14.22	0.76	1018	-	δCH_3(69), δCHI(27)
1006	0.01	1.36	-	-	δCH_3(74)
1000	13.28	19.13	-	1002	δCH_3(48), δCHIV(40)

998	2.24	0.21	-	-	δPhI(53), υPhI(22)
989	28.30	11.85	984	-	δCH_3(59), γCHIV(13)
970	0.09	0.38	-	969	δCH_3(70), υPhI(16)
959	0.05	0.07	956	-	γCHIV(80)
947	0.01	0.01	-	-	γCHI(92)
943	19.10	73.40	-	-	υPhII(28), δCH_2(29), υCN(11)
941	0.16	0.54	-	-	γCHIV(73), τPhIV(15)
930	6.34	0.22	928	928	γCHI(70), τPhI(14)
922	0.08	0.01	-	-	δCH_3(94)
918	3.23	10.57	-	-	υCC(23), δC=O(22)
903	13.00	181.17	-	905	δCH_3(41), υCO(39)
901	1.12	10.36	-	-	υCC(26), δCH_3(45)
895	8.40	0.40	-	-	γCHII(90)
893	1.72	0.99	-	-	δCH_2(77)
891	1.51	8.77	-	-	υCC(50), γCHIII(35)
880	13.31	0.05	875	880	γCHII(79), τPhII(14)
839	1.09	27.75	841	840	δCH_2(38), γCHI(12)
829	24.61	1.53	-	-	γCHIV(81)
824	24.53	8.52	-	-	δPhII(15), υPhI(42), δPhIII(10)
822	0.01	0.43	-	-	γCHI(100)
818	3.39	0.63	-	-	γCHIV(95)
811	1.32	8.25	809	812	υCC_3(52), γCHIV(22)
797	37.46	13.26	-	-	γCHI(42), υCC(17), τPhI(12)
783	9.58	4.61	-	780	γCHI(28), υPhIV(48)
773	39.00	0.12	775	-	γCHII(85)
748	3.01	12.23	750	750	υCC(19), τPhI(23), δCH_2(26)
737	1.55	3.72	-	733	τPhIV(48), γCC(34),

					τPhIII(10)
726	0.73	0.08	728	-	τPhII(53), τPhIII(24), τPhIV(10)
715	0.49	37.45	-	-	δPhIV(37), δPhIII(28)
699	6.67	6.32	703	701	τPhI(62), γCC(18)
692	15.96	0.56	690	-	τPhIII(29), τPhIV(25), τPhII(27)
646	1.33	1.09	644	644	δPhIII(22), τPhI(17), γNH(45)
632	0.20	4.37	-	-	δPhI(77)
626	0.88	8.20	-	-	δPhIV(77)
624	8.82	1.11	-	622	γCN(28), γC=O(24), τPhII(21)
604	9.05	3.52	606	598	δPhII(32), δPhIII(30)
586	1.35	0.10	-	-	γCN(25), γNH(13), γC=O(21), τPhII(17)
562	10.93	15.42	567	560	δCC_3(20), δPhIII(28), δPhI(23)
545	6.86	0.56	547	-	δPhI(46), γCC_3(15)
540	18.09	0.62	-	-	γC=O(43), γNH(28), δCH_2(12)
539	21.90	0.15	-	536	τPhIV(34), γCC_3(45)
527	2.97	4.63	525	524	δPhII(26), δCC_3(34)
502	40.69	1.43	-	499	τPhI(19), γCC_3(39), δPhII(10)
446	1.35	0.75	448	445	δCC_3(62)
437	0.61	1.12	-	-	τPhI(44), γCC_3(17)
429	2.63	1.33	426	426	τPhII(36), τPhIII(28)
413	2.48	0.04	-	-	τPhII(40), τCN(10), γCC_3(11)
400	0.03	0.02	-	-	τPhI(83)

398	0.01	0l01	-	396	τPhIV(80)
384	0.83	2.32	-	-	δCN(22), δPhII(22), δCC_3(35)
374	3.39	1.31	-	375	δCC_3(38), δCN(20)
371	0.13	0.93	-	-	δCC_3(28), τPhIII(24), τPhII(10)
363	0.05	0.18	-	-	δCC_3(29), δPhI(22), τPhII(26)
342	0.16	0.65	-	-	δCC_3(43), τPhII(10)
335	3.74	4.76	-	333	δPhI(18), γCC(14), δCC_3(12), τPhII(15)
318	2.91	0.81	-	-	δCC_3(61), δCN(12)
313	0.01	0.04	-	-	τCH_3(89)
284	1.30	0.78	-	286	δCC_3(42), δCN(21), δCC(15)
280	0.30	0.35	-	-	τPhIV(128), τPhII(29), δCC_3(33)
272	3.38	3.24	-	-	γCC(24), δCC(13), τPhI(10)
269	1.06	0.17	-	-	δCH_2(80)
257	0.15	1.03	-	260	τCH_3(84)
224	0.02	1.26	-	-	τCH_3(59), τPhII(124)
209	1.26	0.59	-	-	δCC(26), δPhIV(22), δCH_2(10)
208	0.01	0.72	-	-	τPhII(38), τCH_3(27)
185	0.87	0.98	-	187	δCC(21), δPhIV(34), δCC_3(14)
176	0.43	1.26	-	170	γCC(22), τPhII(12), δCC_3(11), τPhIII(10), τCH_3(10)
122	1.73	1.04	-	124	τPhI(37), δCH_2(10), δCC(13)
106	0.18	2.35	-	104	δCN(33), δCC(33), τPhI(12)
98	0.09	0.41	-	-	τPhIV(19), τC=O(12),

					τPhIII(19), γCC(17), γNH(10)
61	0.09	0.01	-	-	τCC_3(25), τNH(27)
56	0.85	1.05	-	-	τCH_3(26), τCC_3(22), τCC(14)
53	0.33	0.67	-	-	τCH_3(49), τCC_3(16)
46	0.48	1.09	-	-	δCC(48), γCC(12), δCH_2(11)
45	3.46	1.15	-	-	τNH(24), τCH_2(24), τCC_3(19)
31	1.97	1.74	-	-	τCC_3(22), τCH_2(11), τCC(10), γCC(21)
25	0.35	3.00	-	-	γCC(23), δCH_2(22), δCN(15), δCC(15)
22	0.61	3.80	-	-	τCC_3(20), τCC(34), τC=O(10)
11	0.11	3.71	-	-	τCC(26), τC=O(10), γCC(11), τCC_3(10)
6	0.08	2.64	-	-	τCH_3(25), τCC(25), τC=O(17), τCH_2(10)

---

[a]υ-stretching; δ-in-plane deformation; γ-out-of-plane deformation; τ-torsion; PhI-C_{41}-C_{43}-C_{47}-C_{45}-C_{42}-C_{40}; PhII-C_{29}-C_{27}-C_{25}-C_{26}-C_{28}-C_{31}; PhIII-N_{35}-C_{24}-O_{34}-C_{25}-C_{26}; PhIV-C_1-C_2-C_3-C_4-C_5-C_6.

Table 3

The binding affinity values of different poses of the title compound predicted by AutodockVina.

Mode	Affinity (kcal/mol)	Distance from best mode (Å)	
-	-	RMSD l.b.	RMSD u.b.
1	-8.5	0.000	0.000
2	-8.4	18.347	19.273
3	-8.2	6.757	13.844
4	-8.1	2.722	7.911
5	-8.1	2.179	3.491
6	-8.1	7.309	10.133
7	-7.9	16.684	17.634
8	-7.9	7.387	9.579
9	-7.8	17.063	20.172

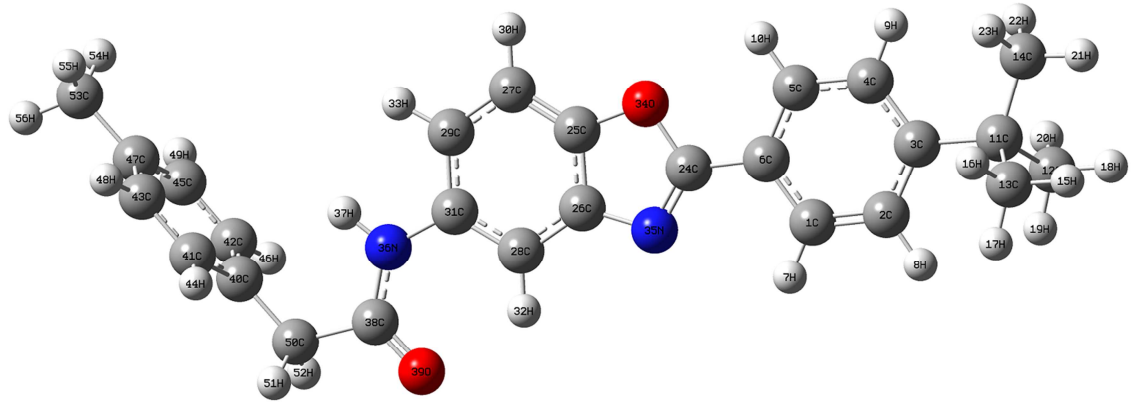

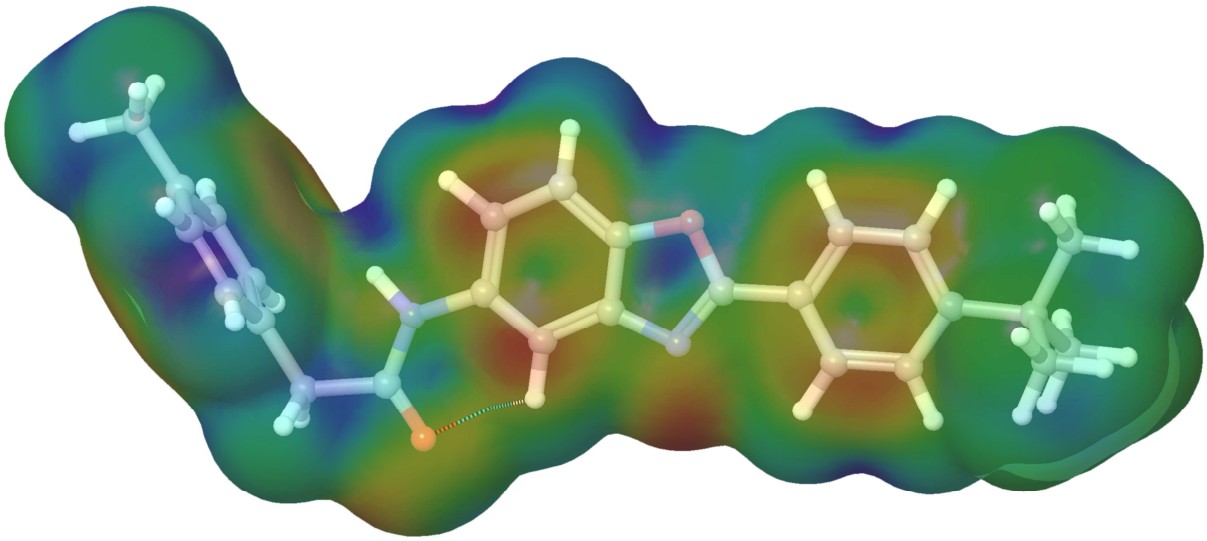

Fig.2 ALIE surface of 5-[(4-methylphenyl)acetamido]-2-(4-tertbutylphenyl) benzoxazole molecule

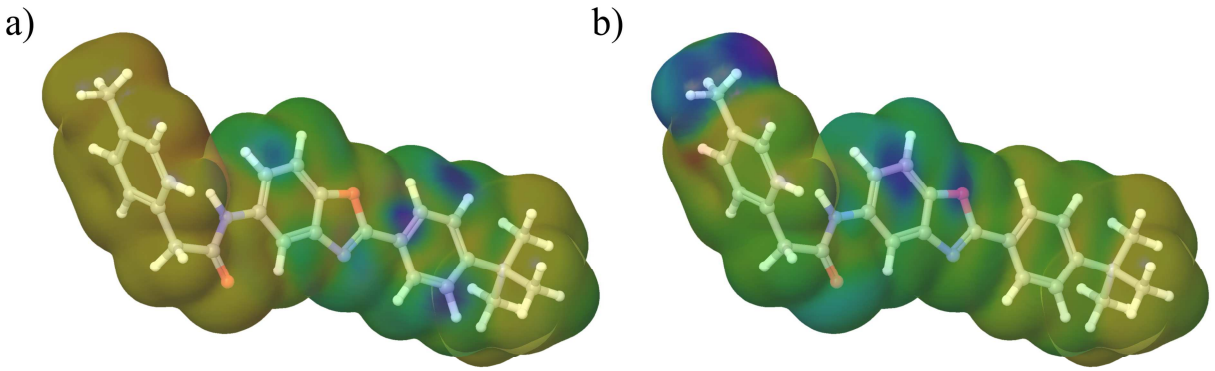

Fig.3 Fukui functions a) f^+ and b) f^- of 5-[(4-methylphenyl)acetamido]-2-(4-tertbutylphenyl) benzoxazole molecule

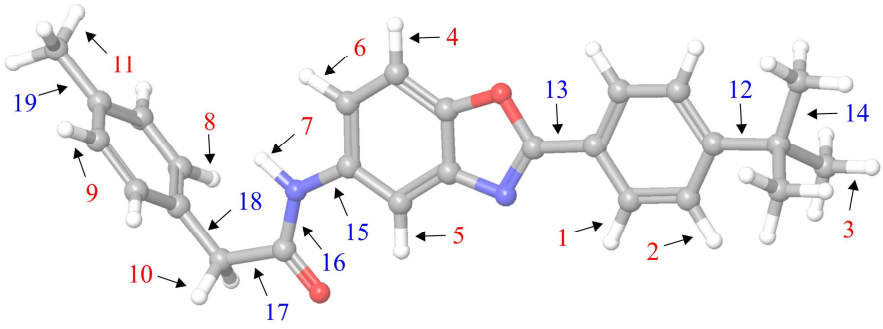

Fig.4 BDEs of all single acyclic bonds of 5-[(4-methylphenyl)acetamido]-2-(4-tertbutylphenyl) benzoxazole molecule

Bond	BDE [kcal/mol]
1	118.94
2	115.63
3	107.62
4	119.23
5	121.88
6	119.70
7	105.84
8	116.95
9	116.96
10	92.68
11	93.96
12	88.91
13	125.71
14	70.52
15	93.50
16	83.09
17	70.18
18	95.33
19	102.92

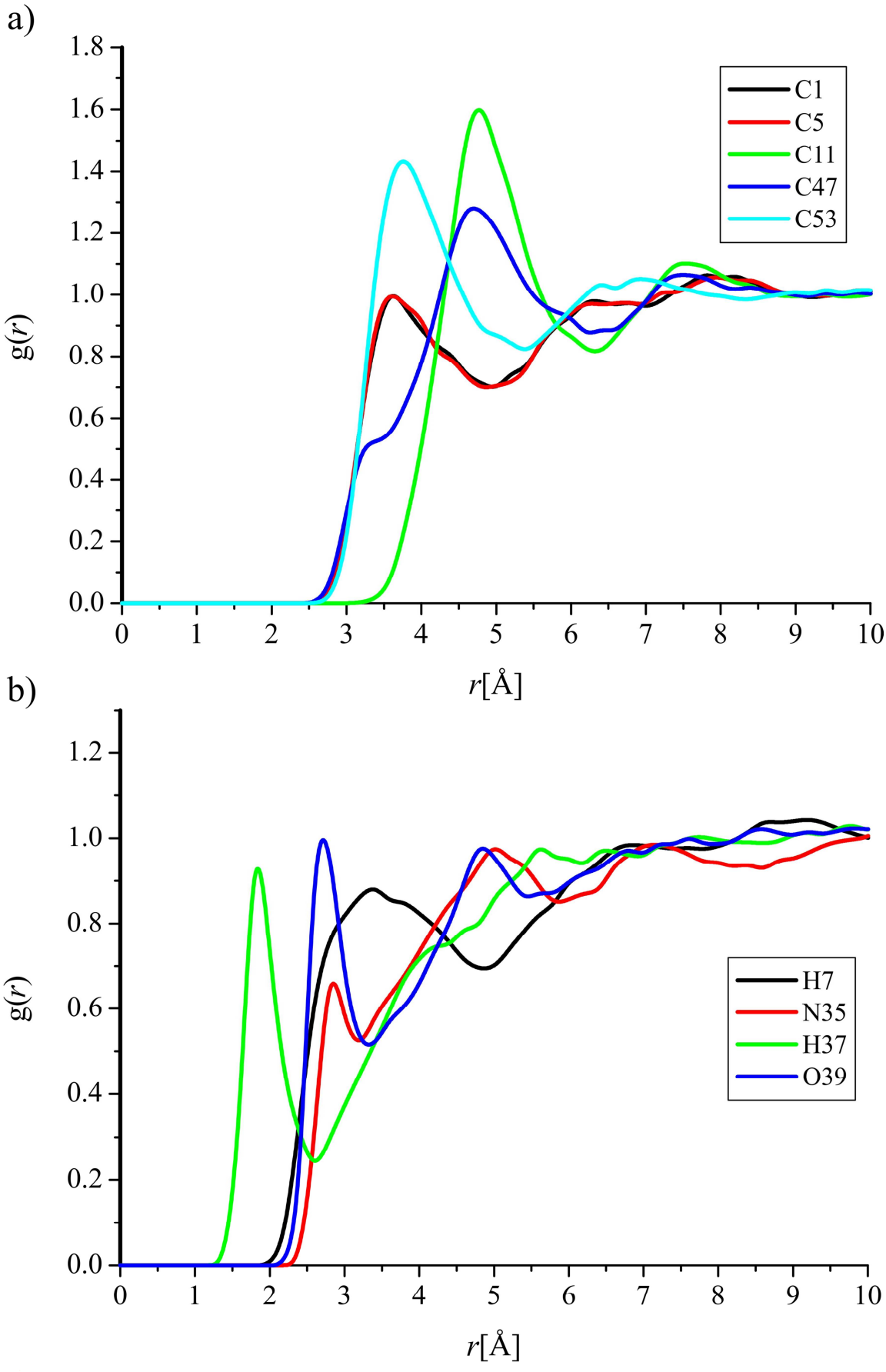

Fig.5 RDFs of atoms of 5-[(4-methylphenyl)acetamido]-2-(4-tertbutylphenyl) benzoxazole with pronounced interactions with water: a) carbon atoms and b) non-carbon atoms

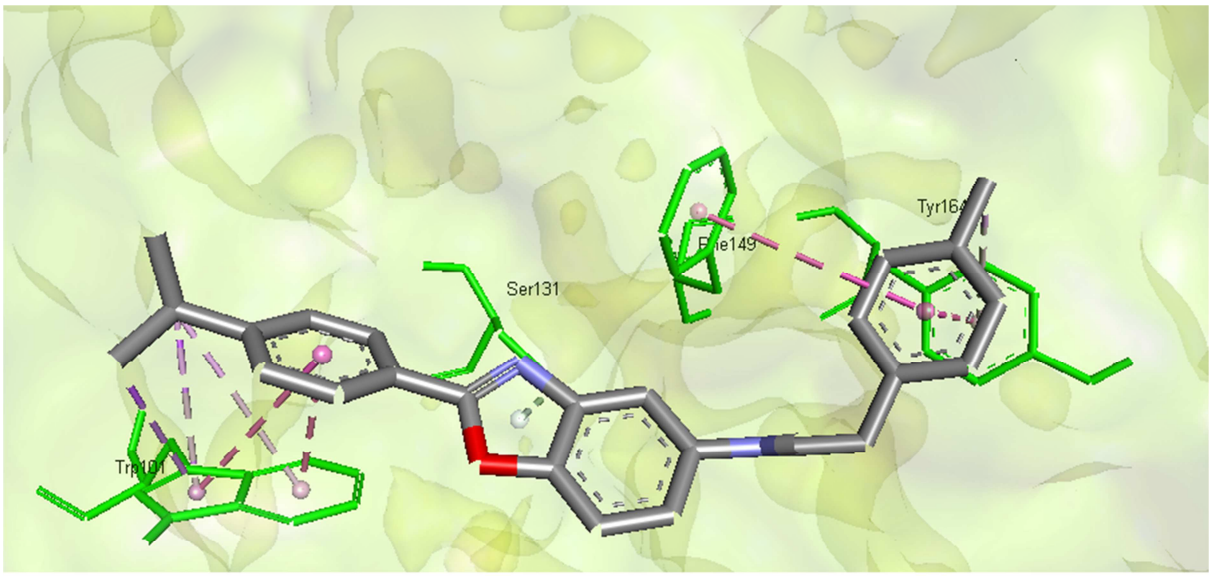

Fig.6 **Amino acids of thymidylate synthase receptor interaction with the docked ligand and receptor surface as background**

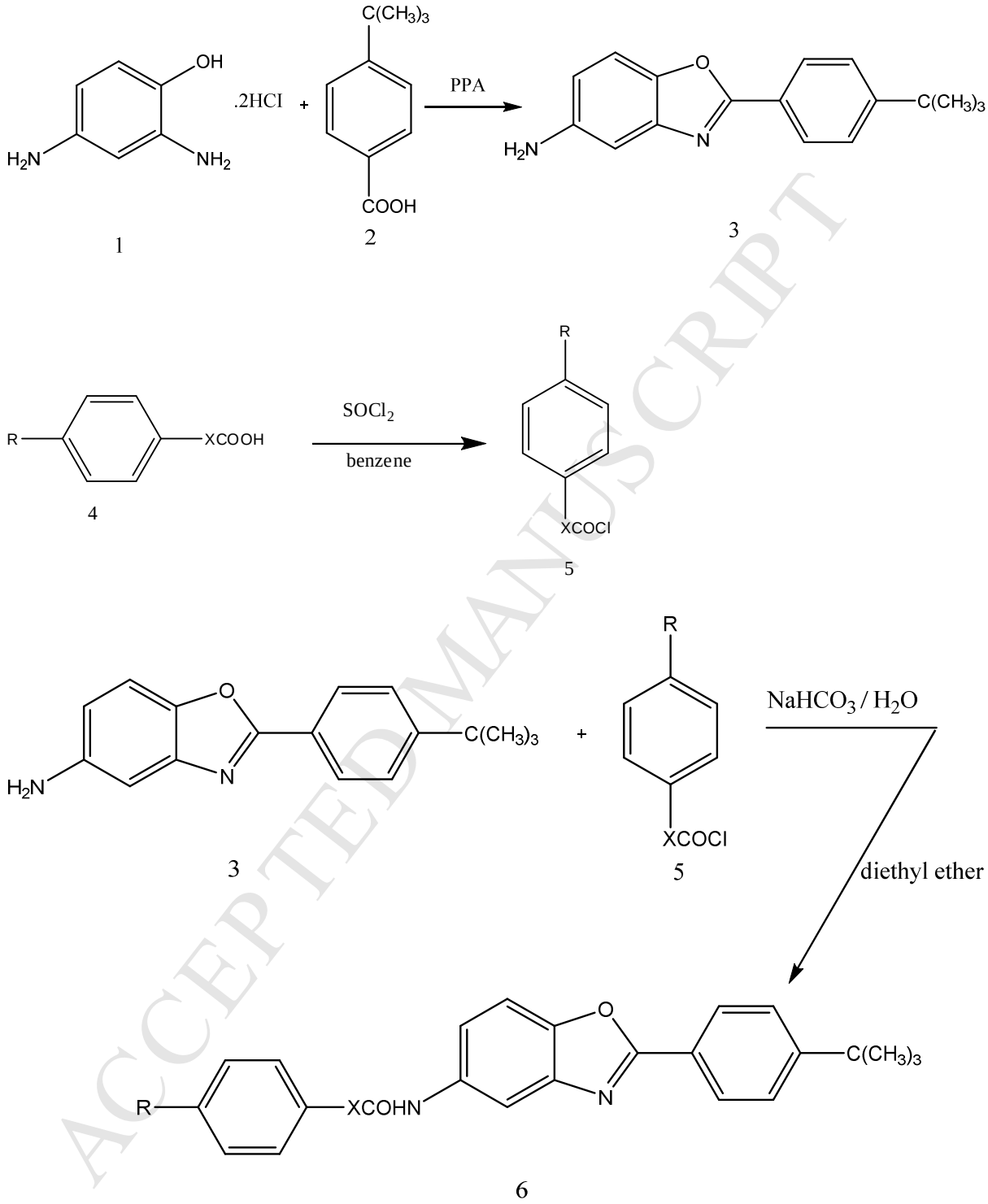

R=CH_3 X=CH_2

Scheme 1. Synthesis of compound 6

Highlights

* IR and Raman spectra were measured
* Exhibits significant antifungal activity
* ALI, BDE, RDF have been discussed in detail
* Docking suggests the title compound as an anti-cancerous drug.